9
Oxygen Ion-Conducting Materials

Vladislav V. Kharton, Fernando M.B. Marques, John A. Kilner, and Alan Atkinson

Abstract

Oxygen ionic and mixed ionic-electronic conductors find important applications in solid-state electrochemical devices, including sensors, solid oxide fuel cells, high-temperature electrolyzers, and oxygen separation membranes. This chapter presents a brief overview of oxide phases with high diffusivity of O^{2-} anions, providing an introduction to this fascinating topic. Particular emphasis is centered on the comparative analysis of ionic and electronic conductivity variations in the major groups of solid oxide electrolytes and mixed conductors, such as perovskite- and fluorite-related compounds, apatite-type silicates, and derivatives of γ-$Bi_4V_2O_{11}$ and β-$La_2Mo_2O_9$. The defect chemistry mechanisms relevant to the oxygen ion migration processes are briefly discussed.

9.1
Introduction

Technologies based on the use of high-temperature electrochemical cells with oxygen anion- or mixed-conducting ceramics provide important advantages with respect to the conventional industrial processes [1–8]. In particular, solid oxide fuel cells (SOFCs) are considered as alternative electric power generation systems due to high energy-conversion efficiency, fuel flexibility, and environmental safety [1–3]. Dense ceramic membranes with mixed oxygen-ionic and electronic conductivity have an infinite theoretical separation factor with respect to oxygen, and can be used for gas separation and the partial oxidation of light hydrocarbons [4, 5, 7, 8] (these and other applications are reviewed in Chapters 12 and 13). For all types of electrochemical cells, the key properties which determine the use of a material are the partial ionic and electronic conductivities. As an example, solid electrolytes for SOFCs, oxygen pumps and electrochemical sensors should exhibit a maximum oxygen ionic conductivity, while the electronic transport should be minimal. In contrast, for SOFC electrodes

Solid State Electrochemistry I: Fundamentals, Materials and their Applications. Edited by Vladislav V. Kharton

ISBN: 978-3-527-32318-0

and oxygen separation membranes, both ionic and electronic conductivities should be as high as possible (see Chapter 3). In the case of SOFC interconnectors, both minimum ionic and maximum electronic conduction are necessary.

In this chapter we present a brief overview of the major groups of solid oxide electrolytes and mixed conductors, placing special emphasis on their ion transport properties. The main features of the crystal structures enabling fast anion diffusion and the basic defect-chemistry mechanisms relevant for these materials are addressed in Chapters 2–4. Since it has been impossible to cover all promising compositions and migration-affecting factors within the chapter, priority has been given to those single-phase oxide ceramics which exhibit a high ionic conductivity sufficient for practical applications. Further information regarding conventional and new materials for high-temperature electrochemical devices is available in a variety of reviews and monographs [4, 6–17].

9.2
Oxygen Ionic Transport in Acceptor-Doped Oxide Phases: Relevant Trends

Perhaps one of the most widely studied topics in high-temperature electrochemistry is the oxygen ion conductivity of the fluorite-structured binary oxide systems. Except for the δ-phase of Bi_2O_3, these are formed by preparing solid solutions of tetravalent metal oxides (e.g., zirconia and ceria) with lower-valent metal oxides, most notably the trivalent rare earths (Ln^{3+}). In these solid solutions, addition of the lower-valent cation is charge-compensated by the formation of oxygen vacancies, which are highly mobile at elevated temperatures. The combination of this ability of the fluorite lattice to accept high concentrations of vacancies with the fact that they are mobile at high temperatures is the origin of this high oxygen ion conductivity. A prominent feature seen in all investigations is the maximum in the conductivity isotherms with respect to the content of the aliovalent additive. A simple analysis [12] shows that a maximum is to be expected when the oxygen sublattice is half occupied, although experimentally this is found to occur at much lower concentrations. As an example, this concentration in $Zr_{1-x}Y_xO_{2-x/2}$ corresponds to $x \approx 0.07$–0.11, depending on temperature, preparation route, pre-history, purity, and other factors. For zirconia, this effect is complicated by the fact that it only adopts the fluorite structure (at moderate temperatures) when the dopant concentration is already high, because the small Zr^{4+} cation (0.84 Å in eightfold coordination) is not large enough to stabilize the fluorite structure to low temperatures. In contrast, in pure ceria the Ce^{4+} cation (0.97 Å in eightfold coordination) is large enough to be stable in the fluorite lattice, and thus provides an ideal opportunity for examining any effects from dilute to concentrated solid solutions. The example of ceria-based electrolytes is used in this section to illustrate the key effects of acceptor-type doping, which are observed in most fluorite- and perovskite-related phases.

For most ionic conductors, the conductivity activation energy (E_a) may be considered to consist of two parts, namely the enthalpy of ion migration (ΔH_m) and any terms caused by the interaction of the point defects and/or by the charge carrier formation. For low concentrations of the trivalent additive in ceria lattice, the

interaction term is thought to be due to the formation of defect associates of the oxygen vacancy with the substitutional cation(s). In a simplest case, this type of defect interaction in yttria-doped ceria can be presented as

$$Y'_{Ce} + V_O^{\bullet\bullet} \leftrightarrow \{Y'_{Ce} V_O^{\bullet\bullet}\}^{\bullet} \tag{9.1}$$

with the association enthalpy ΔH_a. Shown here is the simple dimer, or associated pair, but it should be noted that the concentration of substitutional cations is twice that of the oxygen vacancies, and so there is a high probability of forming trimers and higher clusters as the concentration increases (a point to which we will return). If simple dimers were to form, then the activation energy for conductivity would be given by the sum ($\Delta H_a + \Delta H_m$). Irrespective of the association type, two vacancy concentrations can be defined: the *stoichiometric concentration*, which is determined by the electroneutrality condition; and the *mobile* or "*free*" *vacancy* concentration given by the association equilibria, which can be very different. Only the "free" vacancies are mobile and can contribute significantly to oxygen ionic transport.

What is found by experiment is that, as a general rule, at substitutional concentrations close to the maximum in the conductivity isotherms, there is a minimum in the activation energy. In an early (but very comprehensive) study of ceria solid solutions with the trivalent rare earths, Faber *et al.* [18] showed that the depth of the minimum, and the concentration at which it occurs, depends upon the identity of the rare earth cation (Figure 9.1). The minima have been ascribed [19] to competitive defect interactions. Initially, the effect is a weakening of the association energy of the dimers caused by an electrostatic interaction between the cluster and the unassociated substitutionals having an opposite effective charge in the lattice; note, however, that

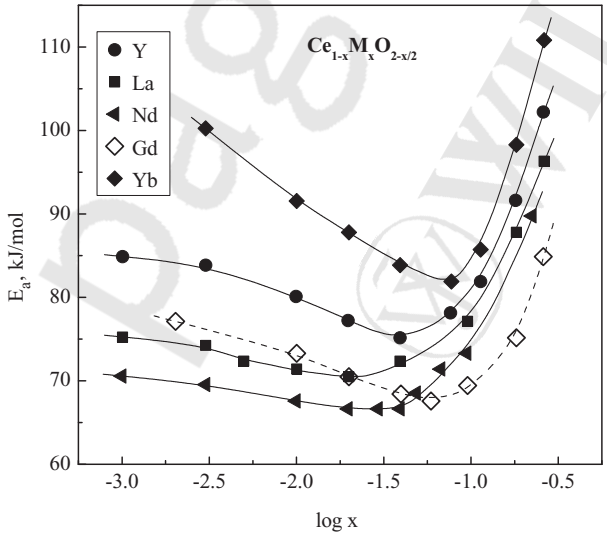

Figure 9.1 Activation energy versus dopant concentration in ceria solid solutions. Data from Ref. [18].

the intrinsic vacancy-formation process cannot be neglected at low dopant concentrations. On further doping, higher-order clusters form, which act as much deeper traps for the oxygen vacancies and thus increase the association term.

There are distinct differences between the compositional dependence of E_a for each of the substitutional species, both in terms of the magnitude and shape of the dependence, even though they have the same effective charge and give rise to identical stoichiometric vacancy concentrations (see Figure 9.1). In particular, there is a further minimum here as a function of the size of the substitutional cation. This is shown much better in Figure 9.2, where the minima with concentration are plotted as a function of the dopant radius. The global minimum corresponding to the lowest total activation energy is an important feature for the technological application of ceria solid solutions. It is usually assumed that, to a first approximation, the migration enthalpy in these materials changes very little from system to system, and that the observed changes in E_a reflect changes in the association term. If this is the case, then Figures 9.1 and 9.2 demonstrate that the association energy must contain terms that reflect both an electrostatic and an elastic interaction between the components of any defect cluster, as the dopant size is so important.

The explanation of the minimum in activation energy with dopant radius was initially made in terms of the elastic component of the association energy of the simple pairs – that is, in terms of the size mismatch between the host and the substitutional ion (see early references in Ref. [12]). Later computer simulations of

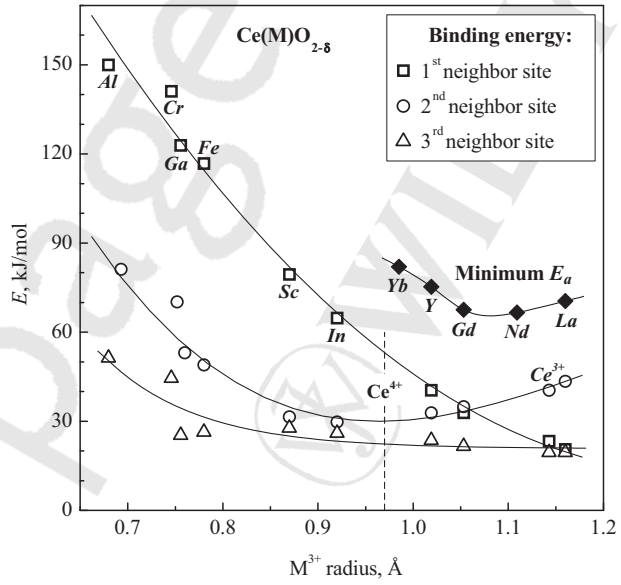

Figure 9.2 The minimum activation energy in ceria-based systems (closed symbols) and calculated binding energies of vacancy substitutional pairs in ceria (open symbols) plotted against the M^{3+} dopant cation radius in eightfold coordination. Data from Refs. [18, 20].

ceria-based solid solutions [20] showed that the situation is more complicated and that, in fact, the minimum is caused by the switchover of the vacancy from a first ($r_{ion} \leq Gd^{3+}$) to a second nearest-neighbor site ($r_{ion} \geq Gd^{3+}$) to the substitutional ion in the fluorite lattice, as the dopant size exceeds that of the host (see Figure 9.2). A similar dependence is operative in zirconia electrolytes [21]; moreover, the same type of size dependence could be found for larger clusters. More recent density functional calculations for ceria-based materials have confirmed this trend [22], and have shown that at the minimum in the association (binding) energy where the crossover takes place, there is a balance between the electrostatic and elastic interactions that removes the energy difference between the first- and second-neighbor configurations. It would seem, therefore, that the above-mentioned theoretical studies present a consistent account of the size dependence. However, recent calorimetric studies performed by Navrotsky *et al*. [23] have shown that this explanation might not yet be complete. In fact, their measurements would indicate that the vacancy is, as expected, in the first nearest-neighbor position in CeO_2-Y_2O_3, and CeO_2-Gd_2O_3, but the same seems to be true for CeO_2-La_2O_3 solid solutions, in contrast to the calculated predictions.

A word of caution is needed at this point on the above observations and following comments. It is clear from Figure 9.1 that the defect structure has a strong concentration dependence, and thus for meaningful comparisons between different materials it is necessary to compare like with like. However, the concentration dependence of the activation energy curve is different for each substitutional cation; indeed, Andersson *et al*. [22] showed that the interplay between the electronic and elastic component depends heavily on the dopant type. It is probably the case that the type of defect clusters observed is very dependent upon concentration, and that typically around the concentration for the minimum activation energy a change in the defect structure takes place.

In the case of mixed ionic-electronic conductors, an analysis of the lattice strain-promoted clustering phenomena becomes even more complicated as the oxygen vacancy concentration – and, consequently, the ionic conductivity – depend on both the oxygen partial pressure and cation size mismatch. In this situation, any quantitative comparison is often difficult, even when the experimental data were obtained for essentially similar materials and under identical external conditions. Nonetheless, the data available on ferrite-, cobaltite-, and nickelate-based systems with perovskite-related structures (e.g., [24–28]) seem to confirm that, when long-range ordering in the oxygen sublattices can be neglected, the ionic transport tends to increase with decreasing difference between the host and dopant cation sizes. As an example, Figure 9.3 compares the variations of partial ionic and p-type electronic conductivities in perovskite-type $Ln_{0.5}A_{0.5}FeO_{3-\delta}$ (A = Sr,Ba) [24]. Under oxidizing conditions, increasing the mismatch between Ln^{3+} and A^{2+} radii weakens the metal–oxygen bonding, increases the oxygen nonstoichiometry, and decreases the hole concentration due the electroneutrality condition; the ionic transport then exhibits a trend opposite to the vacancy concentration variations. A similar tendency is observed for the ionic conductivity in reducing atmospheres, when the oxygen deficiency becomes similar for all $Ln_{0.5}A_{0.5}FeO_{3-\delta}$ perovskites; the activation energy

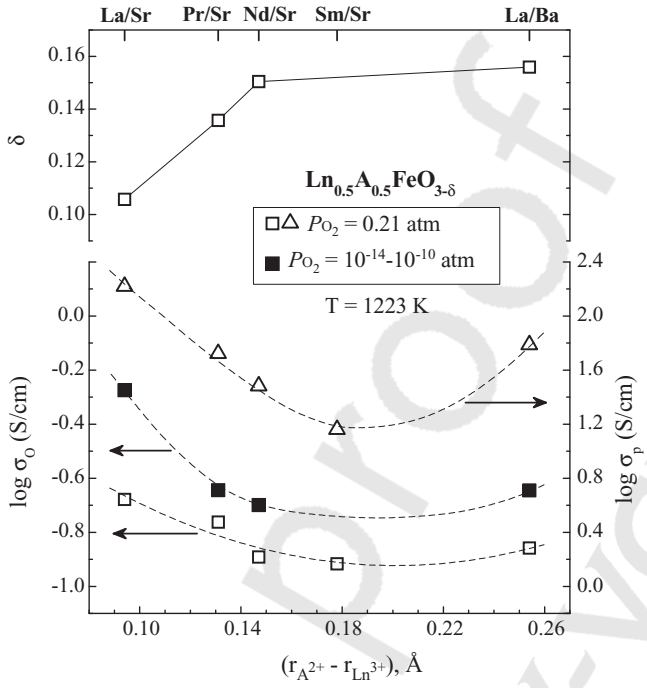

Figure 9.3 Oxygen nonstoichiometry at atmospheric oxygen pressure (top), and values of partial p-type electronic and ionic conductivities in air, and ionic conductivity in reducing atmospheres when the oxygen content in the perovskite lattice $(3-\delta)$ is close to 2.75 atoms per formula unit (bottom), versus the difference between A^{2+} and Ln^{3+} cation radii in $Ln_{0.5}A_{0.5}FeO_{3-\delta}$ (Ln = La-Sm, A = Sr, Ba) at 1223 K. Data from Ref. [24]. All A-site cation radii correspond to ninefold coordination.

increases with lattice strains and displays no direct correlations with the stereological parameters which might affect ion diffusivity [24].

One way to confirm the defect cluster configurations is to use localized probes such as the synchrotron-based extended X-ray absorption fine structure (EXAFS) and X-ray absorption near edge structure (XANES) spectroscopic analyses to examine the local cation coordination [29, 30]. Alternatively, electron beam-based techniques such as high-resolution electron energy loss spectroscopy (EELS) and selected-area electron diffraction (SAED) can be used [31]. Most of these techniques have been applied to materials with the acceptor-type dopant concentration >5%, where trimers and higher-order clusters are to be expected. Interestingly, even in concentrated solid solutions based on ceria, the different trivalent substitutionals show differing behaviors. The study of yttria- and gadolinia-doped $CeO_{2-\delta}$ using EXAFS and XANES [29] revealed a greater tendency towards defect association in the former system, with the most likely configurations comprising either two or four trivalent cations clustered with one or two neighboring oxygen vacancies. Similar conclusions were drawn when the study was extended to the CeO_2-La_2O_3 system [30]. Deguchi *et al.* [30] also suggested a similarity between the radial distribution functions for the

dopant cations (e.g., R_{Ln-Ln}) and those found in the corresponding rare earth sesquioxides, concluding that "*. . .it is interesting to note that the original structure of each dopant oxide is kept even in the ceria lattice*". This theme was echoed by Ou *et al.* [31], who showed that the defect structure in ceria electrolytes does indeed change with the dopant content, albeit for rather concentrated materials containing 15–25% additives; these authors proposed the existence of ordered nanodomains – essentially large vacancy-dopant clusters that resemble the parent C-type structure of Ln_2O_3.

Some final comments are needed to qualify the previous analysis. For the experimental observations, it has already been stated that care must be taken to ensure that like materials are compared (although the term "like" materials is not quite clear). It is also instructive to remember that the different techniques probe the materials over different length scales, and are sensitive to the different properties of the material. The theoretical techniques also differ in their strengths and weaknesses to simulate these complex lattices, and will be more successful in their description of one aspect of the problem. However, the most problematic issue is the comparability of even the most "identical" samples.

In most oxygen ion-conducting materials used for practical applications, the lattice diffusivity of the cations is particularly sluggish. This brings its own problems for understanding the microscopic mechanisms and materials optimization. Usually, the distribution of dopant cations is assumed to be random among the available lattice sites – indeed, this is the aim of the (mainly solution based) fabrication processes designed to maximize cation mixing. Yet, this is far from the case in the ceramic samples that are subsequently investigated. The computer simulations show that there is an energetic advantage for the formation of clusters. However, these need to form from the initial random distribution imposed by fabrication and thermal prehistory; the redistribution kinetics may be very slow, and it is unlikely that a true "equilibrium" structure will result. Whichever metastable cation distribution results from the prehistory, the oxygen sublattice will rapidly adjust to it. It is probable, therefore, that subtle differences in the observed defect cluster structure can occur between ostensibly similar materials, and this should be taken into account when evaluating the experimental data relating to this fascinating topic.

9.3
Stabilized Zirconia Electrolytes

The maximum ionic conductivity in ZrO_2-based systems is observed when the content of acceptor-type dopant cations with the smallest radii (Sc, Yb, Y) is close to the minimum necessary to completely stabilize the cubic fluorite-type phase in the operating temperature range [9, 11, 16, 32–35]. This concentration (often referred to as the low stabilization limit) and the conductivity of the ceramic electrolytes are dependent, to a finite extent, on the pre-history and various microstructural features. In addition to the metastable states discussed above, critical microstructural factors

include the dopant segregation at grain boundaries, impurities, porosity, and the formation of ordered microdomains. Nevertheless, despite minor contradictions still existing in the literature, for most important systems the dopant concentration ranges providing maximum ionic transport are well established. For example, the highest conductivity in $Zr_{1-x}Y_xO_{2-x/2}$ and $Zr_{1-x}Sc_xO_{2-x/2}$ is observed at $x =$ 0.07–0.11 and 0.09–0.11, respectively. Although further additions decrease the ionic conduction due to progressive defect clustering, typical dopant concentrations in the solid electrolyte ceramics used for most practical applications are moderately higher, for example, $x \approx 0.15$ in $Zr_{1-x}Y_xO_{2-x/2}$ (8 mol.% Y_2O_3). This doping strategy aims, in particular, to partly suppress ageing at 900–1300 K associated with kinetically limited phase changes and time degradation of the conductivity. In the case of scandia-stabilized zirconia (SSZ), where a relatively fast decomposition of metastable cubic and rhombohedral solid solutions and/or partial ordering occur at moderate temperatures, this strategy is less effective compared to Y-containing analogues. Taking into account the precursor costs, yttria-stabilized zirconia (YSZ) is among the most commonly used solid electrolytes to date. Numerous attempts have been made to identify new electrolyte compositions in ternary systems, particularly to increase the conductivity by optimizing the average size of dopant cations, to increase the stability of Sc-containing materials by co-doping, or to decrease the cost of Ln^{3+}-stabilized phases by mixing rare- and alkaline-earth dopants [33]. However, no worthwhile improvement has been observed. Figure 9.4a displays typical values of the total conductivity (predominantly ionic) for selected ZrO_2-based phases and one YSZ-Al_2O_3 composite. Small additions of highly dispersed alumina make it possible to improve the mechanical strength and to reduce the grain-boundary resistance due to the "scavenging" of silica-rich phases [45–47]; this approach has been used successfully to prepare a variety of solid electrolyte ceramics (e.g., [48–50]).

Another necessary comment is that, if compared to other oxide electrolytes, stabilized zirconia ceramics without variable-valence additives exhibit, as an average, a minimum electronic contribution to total conductivity in the oxygen partial pressure range most important for practical applications [1, 6, 10, 11, 13, 14, 16, 33]. This approximate P_{O_2} range is from 100–200 atm (oxygen compressors, impurity sensors in oxygen, high-pressure SOFCs) down to 10^{-25}–10^{-20} atm (standard SOFC systems, water vapor electrolyzers, exhaust gas sensors). Whilst in reducing environments, the n-type electronic transport in ThO_2- and $LaGaO_3$-based electrolytes is lower than that of stabilized ZrO_2 zirconia, the latter shows lower p-type electronic conduction and, thus, a higher performance under oxidizing conditions. It should be noted also that the performance of lanthanum gallate at low P_{O_2} is limited by Ga^{3+} reduction and gallium oxide volatilization, rather than the n-type electronic conductivity. For applications in oxygen-separation membranes and SOFC electrodes, the electronic transport in stabilized zirconias can be moderately enhanced by incorporating variable-valence cations (e.g., Ti, Nb, Cr, Tb, Pr) into the fluorite-type lattice [4, 9, 17, 33, 51, 52]. However, such doping leads usually to decreasing ionic conductivity; the solubility of transition metal cations is relatively low and temperature-dependent, whereas the addition of praseodymium oxide causes thermomechanical instability.

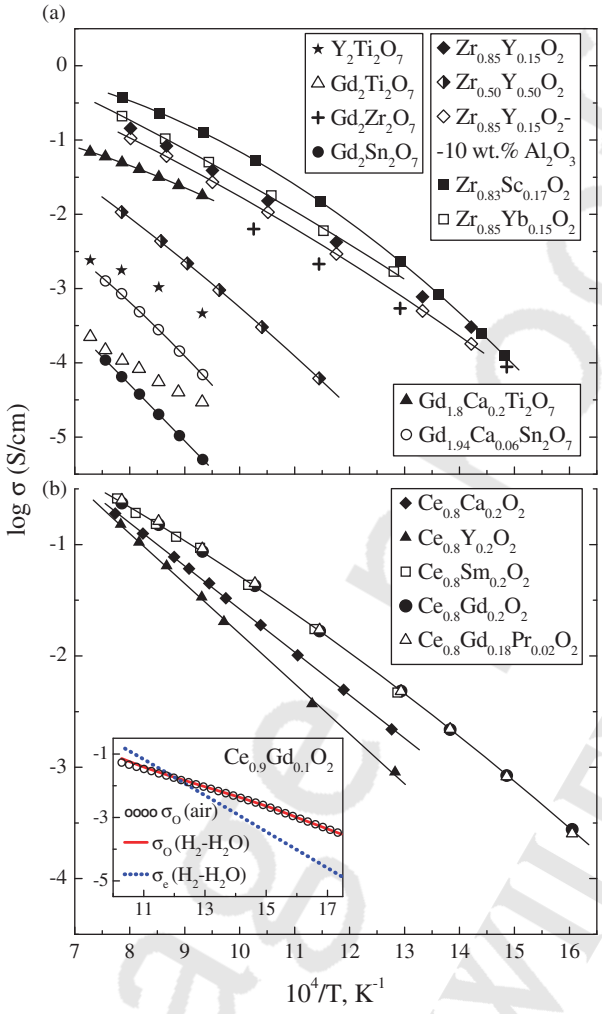

Figure 9.4 Total conductivity of stabilized zirconia (a) and doped ceria (b) solid electrolytes [34–40], compared to the oxygen ionic conductivity of pyrochlore-type $Gd_2Zr_2O_{7-\delta}$ [41], $(Gd,Ca)_2Ti_2O_{7-\delta}$ [42], $(Gd,Ca)_2Sn_2O_{7-\delta}$ [43], and $Y_2Ti_2O_{7-\delta}$ [44]. All data correspond to the atmospheric oxygen pressure. The inset shows the ionic conductivity of $Ce_{0.9}Gd_{0.1}O_{2-\delta}$ in air, and the partial ionic and electronic conductivities in a reducing atmosphere containing 10% H_2 and 2.3% H_2O [14].

9.4 Doped Ceria

The main advantages of fluorite-type $Ce(Ln)O_{2-\delta}$ [38, 53–61] include a faster oxygen-ionic transport with respect to stabilized ZrO_2, a lower cost than that of La(Sr)Ga(Mg)$O_{3-\delta}$ (LSGM) ceramics, and modest reactivity and volatility of the components in

comparison with $LaGaO_3$-, $La_{10}Si_6O_{27}$-, and Bi_2O_3-based materials. In addition, the superior catalytic properties of ceria are advantageous for increasing the exchange currents of the SOFC anodes. Among CeO_2-based phases, the highest level of ionic conduction is characteristic of the solid solutions $Ce_{1-x}M_xO_{2-\delta}$ (M = Gd or Sm; $x = 0.10$–0.20) and their analogues obtained by co-doping, where the concentrations of substitutional cations are adjusted to optimize the average radius and hence, to minimize the tendency to vacancy clustering. Selected data on the total conductivity, which is predominantly ionic under oxidizing conditions, are shown in Figure 9.4b. As with all ceramic electrolytes, the grain boundaries are partially blocking to ionic transport across them; this is an extra contribution to the total resistance that is dependent on impurities and dopants that segregate to the boundaries, and is therefore highly variable from one source to another. This has been an origin of numerous contradictions in the reported data, particularly that relating to the optimum ceria-based compositions. Thus, while $Ce_{0.9}Gd_{0.1}O_{1.95}$ has the highest lattice conductivity, $Ce_{0.8}Gd_{0.2}O_{1.90}$ often has higher total conductivity because its grain boundary contribution seems to be more tolerant to impurities [57]. Due to the dopant segregation and interaction with impurities, analogous discrepancies can also be found on the effects of co-doping (e.g., Refs [60–62] and references cited therein).

The p-type electronic conductivity of gadolinia-doped ceria (CGO) in air is 0.5 to 3.0-fold lower than that of LSGM, and this difference increases with decreasing temperature (Figure 9.5). The main problems in using doped ceria as an SOFC electrolyte arise, however, from the partial reduction of Ce^{4+} to Ce^{3+} under the reducing conditions of the anode [11, 13, 16, 55, 57, 69]. This has two main effects: (i) it produces n-type electronic conductivity, which causes a partial internal electronic short circuit in a cell; and (ii) it generates oxygen deficiency and an expansion of the lattice, which can lead to mechanical failure. For $Ce_{0.9}Gd_{0.1}O_{2-\delta}$, the electronic conductivity at the anode side is greater than the ionic conductivity for temperatures higher than about 823 K (inset in Figure 9.4). Such properties mean that ceria electrolytes are viable only for low-temperature operation; at the same time, the appearance of significant mixed conductivity in reducing environments is advantageous for ceria-containing anodes. The behavior of doped $CeO_{2-\delta}$ with respect to variable-valence additives which have been incorporated to further enhance electronic transport in electrodes and ceramic membranes, is generally similar to other fluorite-type oxides, such as zirconia [4, 7, 8, 17, 40, 70–73]. In particular, maximum oxygen permeability is achieved in those systems with the highest solubility of variable-valence cations, such as $Pr^{4+/3+}$ [73]; however, the thermomechanical stability of such ceramic materials remains an open issue.

9.5 Anion Conductors Based on Bi_2O_3

Oxide phases derived from Bi_2O_3 are particularly interesting due to their high ionic conductivity in comparison to other solid electrolytes [4, 74–78]. The maximum ionic transport is known for stabilized δ-Bi_2O_3 with a highly oxygen-deficient fluorite

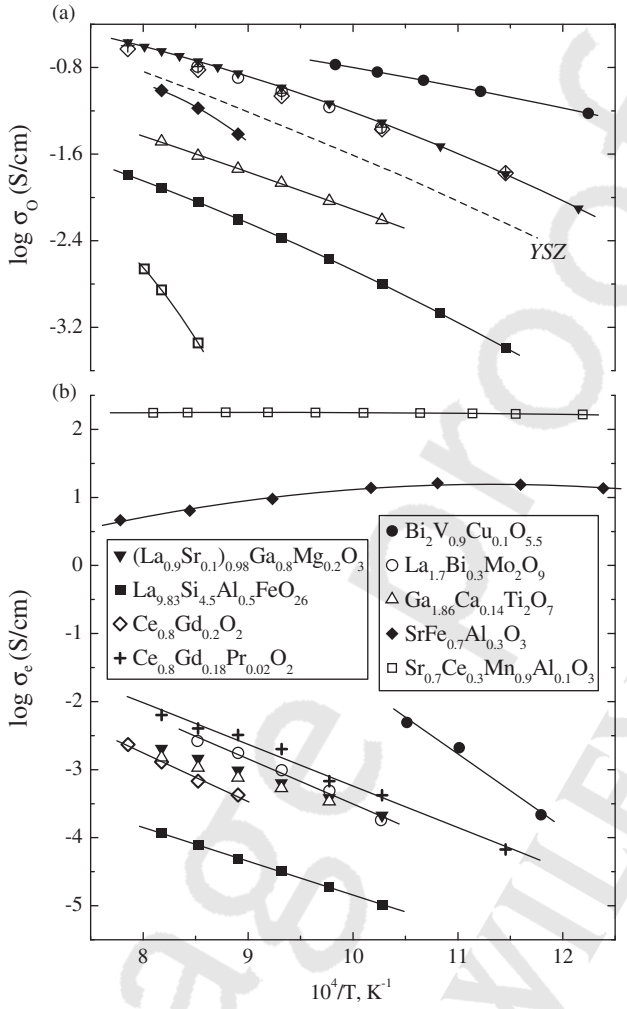

Figure 9.5 Comparison of the oxygen ionic (a) and electronic (p- and n-type) (b) conductivity of selected solid electrolytes and mixed conductors under oxidizing conditions. The partial ionic conductivity of perovskite-type $Sr_{0.7}Ce_{0.3}Mn_{0.9}Al_{0.1}O_{3-\delta}$ [63] correspond to the oxygen partial pressure gradient of 0.21/0.021 atm; data on electronic conduction in $Ce_{0.8}Gd_{0.18}Pr_{0.02}O_{2-\delta}$ [40], $Bi_2V_{0.9}Cu_{0.1}O_{5.5-\delta}$ [64] and $La_{1.7}Bi_{0.3}Mo_2O_9$ [65] correspond to the P_{O_2} range of 1.0/0.21 atm. All other data [36, 40, 64–68] correspond to $P_{O_2} = 0.21$ atm. The ionic conductivity of 8 mol% yttria-stabilized zirconia (*YSZ*) [36] is shown for comparison.

structure, and for one member of the Aurivillius series, γ-$Bi_4V_2O_{11}$, which is the parent compound of the so-called BIMEVOX family. Unfortunately, Bi_2O_3-based materials exhibit a number of disadvantages that hamper their practical application, notably a very high thermal expansion, instability in reducing atmospheres, volatilization of bismuth oxide, a high corrosion activity, and low mechanical strength.

Stabilization of the high-diffusivity δ-Bi_2O_3 phase down to intermediate and low temperatures can be achieved by doping with rare-earth and/or higher-valency cations, such as Y, Dy, Er, W, or Nb [11, 13, 74–76]. Figure 9.6 displays representative data on the total conductivity (mainly ionic) for two δ-Bi_2O_3-based compositions. As with zirconia and hafnia electrolytes, the highest ionic transport is observed for materials containing the minimum addition necessary to stabilize the δ-polymorph; further doping decreases oxygen ion mobility due to a decreasing unit cell volume and increasing the average energy of the metal–oxygen bonding. As Bi^{3+} cations are relatively large, at a given doping level the ionic transport increases with increasing Ln^{3+} radius. However, the minimum stabilization limit also increases with Ln^{3+} size, and this leads to a decrease in the maximum ionic conductivity with increasing radius of the stabilizing cation. As a result, the highest conductivity in the Bi_2O_3-Ln_2O_3 systems is observed for Er- and Y-containing solid solutions, namely $Bi_{1-x}Er_xO_{1.5}$ ($x \approx 0.20$) and $Bi_{1-x}Y_xO_{1.5}$ ($x = 0.23$–0.25). It should be noted, however, that all known δ-Bi_2O_3-based phases with the disordered fluorite structure are metastable at temperatures below 770–870 K, and exhibit a slow degradation in conductivity with time due to sluggish polymorphic transformations. The solid

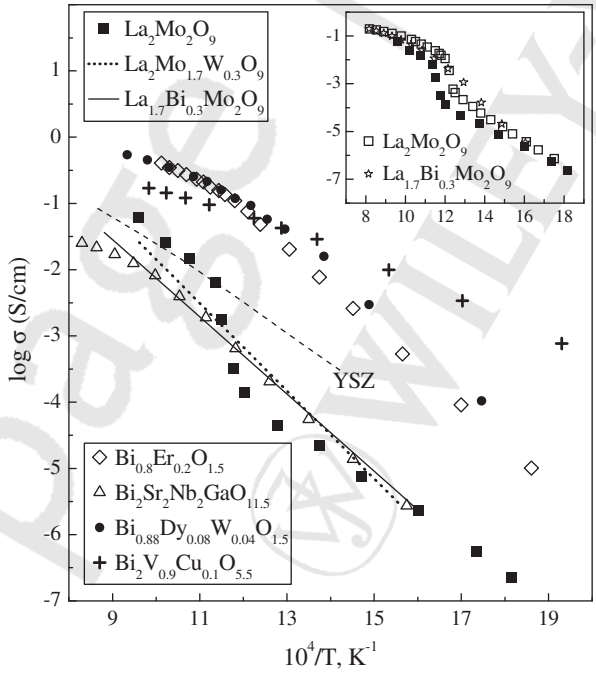

Figure 9.6 Total conductivity of Bi_2O_3-based [64, 75, 79, 80] and $La_2Mo_2O_9$-based [81] materials in air, compared to the ionic transport in 8 mol% yttria-stabilized zirconia (YSZ) [36]. The inset presents the conductivity data on undoped $La_2Mo_2O_9$ and $La_{1.7}Bi_{0.3}Mo_2O_9$ [65], for comparison.

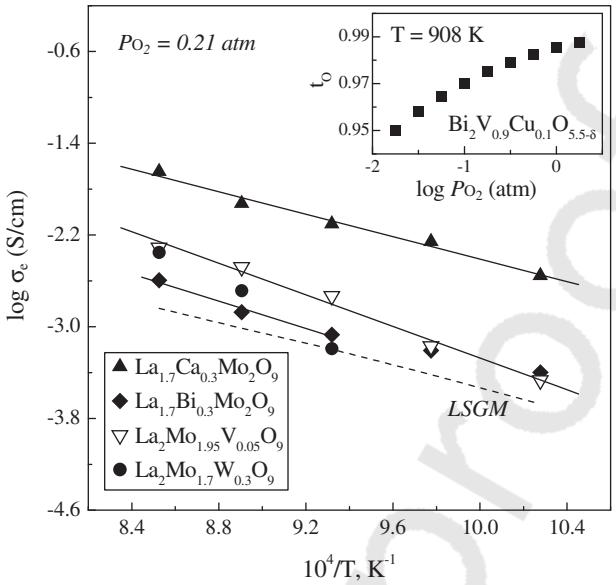

Figure 9.7 Temperature dependence of the electronic conductivity of $La_2Mo_2O_9$-based ceramics, determined by the faradaic efficiency and total conductivity measurements at atmospheric oxygen pressure [65]. The dashed line corresponds to the p-type electronic conductivity of $(La_{0.9}Sr_{0.1})_{0.98}Ga_{0.8}Mg_{0.2}O_{3-\delta}$ (LSGM) electrolyte in air [66]. The inset shows the oxygen partial pressure (P_{O_2}) dependence of the ion transference numbers of $Bi_2V_{0.9}Cu_{0.1}O_{5.5-\delta}$ at 908 K [64].

solutions based on γ-$Bi_4V_2O_{11}$ [49, 77, 78, 82, 83] stabilized by the substitution of 7–15% vanadium with transition metal cations such as Cu, Ni, or Co, possess a better phase stability at moderate temperatures, superior ionic conductivity and oxygen ion transference numbers (t_0) close to unity below 900 K under oxidizing conditions (Figures 9.5 and 9.6). The electrolytic domain of BIMEVOX ceramics is, however, very narrow. For example, decreasing the P_{O_2} to 10^{-2} atm results in the electron transference numbers of $Bi_2V_{0.9}Cu_{0.1}O_{5.5-\delta}$ increasing to 0.05 at 908 K (inset in Figure 9.7); any further reduction will cause phase decomposition.

9.6
Transport Properties of Other Fluorite-Related Phases: Selected Examples

The pyrochlore-type compounds, where the crystal structure is usually considered as a cation-ordered fluorite derivative with $^1/_2$ vacant oxygen site per fluorite formula unit, constitute another large family of oxygen anion conductors [9, 33, 41–43, 84–88]. The unoccupied sites provide pathways for oxygen migration; furthermore, the $A_2B_2O_{7\pm\delta}$ pyrochlore structure may tolerate formation of cation and anion vacancies, doping in both cation sublattices, and antistructural cation disorder. Regardless of these factors,

the oxide pyrochlores possess, in general, worse transport properties compared to the fluorite-type compounds (Figures 9.4 and 9.5). At elevated temperatures (typically up to 1650–2500 K), most pyrochlores disorder into fluorite polymorphs. A decreasing A-site cation radius favors this transition. As a rule, partially cation-disordered pyrochlores exhibit relatively high activation energies for anion transport in the intermediate-temperature range; the maximum ionic conductivity (which can be further enhanced by acceptor-type doping within the solid solution formation limits) occurs for cation stoichiometry, for example, $Gd_2Ti_2O_7$ and $Gd_2Zr_2O_7$. Until now, the highest values of oxygen ion diffusivity in pyrochlore-type compounds have been achieved for $Gd_{2-x}Ca_xTi_2O_{7-\delta}$ with $x \approx 0.2$ [42, 84]. These materials also display a significant electronic contribution to the total conductivity under oxidizing and strongly reducing conditions, close to the upper limit acceptable for solid electrolytes (Figure 9.5). However, due to the limited solubility of variable-valence cations in most pyrochlore phases, the electronic transport cannot be further enhanced by doping to a substantial extent, as for the fluorite-type solid electrolytes.

Among other ion-conducting phases with fluorite-like structures, note should be taken of $Y_4NbO_{8.5}$, $(Y,Nb,Zr)O_{2-\delta}$ solid solutions, and their derivatives (see Refs. [89–91] and references cited therein). The total conductivity of $Y_4NbO_{8.5-\delta}$ is essentially independent of the oxygen partial pressure, which may suggest a dominant ionic transport [90]. However, the conductivity level in this system is rather low, and similar to that in pyrochlore-type titanates and zirconates, although some improvements can be achieved by the addition of zirconia.

9.7
Perovskite-Type $LnBO_3$ (B = Ga, Al, In, Sc, Y) and their Derivatives

Perovskite-type phases derived from $LaGaO_3$ via acceptor-type doping into both cation sublattices of the ABO_3 perovskite structure exhibit a higher ionic conductivity than that of stabilized zirconia, and are thus promising materials for electrochemical cells operating in the intermediate-temperature range (Figures 9.5, 9.8 and 9.9). In oxidizing atmospheres, the p-type electronic transport in the gallate solid electrolytes is moderately higher with respect to CeO_2-based solid solutions (Figure 9.5), but the electrolytic domain of doped $LaGaO_3$ extends to substantially lower oxygen chemical potentials. Following the principle of minimum strain giving maximum oxygen ion mobility, doping with Sr^{2+} leads to a higher ionic conductivity in comparison with either Ca^{2+} or Ba^{2+} [104–106]. As for the fluorite-type electrolytes, there is an optimum concentration of acceptor cations, depending on their size; further additions result in progressive vacancy association processes. In the case of the $La_{1-x}Sr_xGa_{1-y}Mg_yO_{3-\delta}$ (LSGM) series, the maximum ionic transport is achieved at $x = 0.10$–0.20 and $y = 0.15$–0.20, whilst the introduction of smaller Ln^{3+} cations and the creation of an A-site deficiency decrease the ionic conduction [103–108]. It should be noted that qualitatively similar trends are known for numerous perovskite-type systems with either predominant ionic transport or mixed conductivity, such as rare-earth aluminates [109, 110], ferrites, and cobaltites [24–28, 98, 102, 111],